Tabriz Journal of Electrical Engineering (TJEE), vol. 53, no. 4, Winter 2023 Serial no. 106
DOI: 10.22034/tjee.2023.55940.4604

Improving Resilience Based on Proactive Scheduling Management in Multi-energy Carrier Distribution Network Using Microgrids

Behzad Taghipour Moazzen, Maziar Mirhosseini Moghaddam*, Alireza Sahab

Department of Electrical Engineering, Lahijan branch, Islamic Azad University, Lahijan, Iran
email: Behzad.Taghipour@iau.ac.ir, Maziar.Mirhosseini@iau.ac.ir, Alireza.Sahab@iau.ac.ir

Received: 04/04/2023, Revised:09/07/2023, Accepted: 14/10/2023.

Abstract
In recent years, due to the interconnectedness and stress on power distribution and natural gas networks, enhancing the level of resilience against severe natural events such as storms has become crucial and vital. The presence of energy storage systems in microgrids has transformed them into reliable resilience sources in electric energy distribution systems. In this regard, studying the improvement of resilience in distribution networks in the presence of microgrids holds special importance. The objective of this article is to achieve the maximum utilization of available network storage to supply critical and non-critical electrical loads while minimizing the loss of load prior to the occurrence of severe events. To this end, a multi-objective optimization algorithm, namely Ant Colony Optimization, has been employed for proactive scheduling and achieving optimal decisions within consecutive time periods. Simulation results demonstrate that increasing the number of microgrids and expanding energy storage systems in the network not only improves network laudability but also reduces the amount of lost load by 15.27%, thereby increasing the level of resilience.

Keywords
Distribution System Resilience, Multi-Energy System, Proactive Scheduling Management, Microgrids

1. Introduction

During the recent years, resilience has become one of the main keywords in power systems researches with widespread blackouts in all over the world after the occurrence of low-probability and high-impact events such as floods, storms, or earthquakes [1]. Resilience in power systems includes resistance and ability of the system in fast restoration from events such as tsunamis, earthquakes, or cyber-attacks. This study seeks to investigate the effects of hurricanes on resilience.

Resilience of a system is the ability to withstand, survive, and rapidly recover from a severe incident. Typically, the performance of a system is represented by a resilience curve in the form of a trapezoid, as shown in Fig. 1, which depicts the system's performance level during different stages of resilience (avoidance, survival, and recovery). In the time interval from T0 to T1, the system operates in its normal state, and predictive, preparatory, and preventive measures can be taken during this period to mitigate disruptions. T1 represents the occurrence time of the event. Resilience characteristics during the survival stage prevent an immediate decline in system performance, and adaptive measures are taken from T2 to T3 to protect critical loads. Finally, during the recovery stage (T3 to T4), restorative measures are implemented to quickly restore interrupted loads and repair or replace vulnerable equipment.

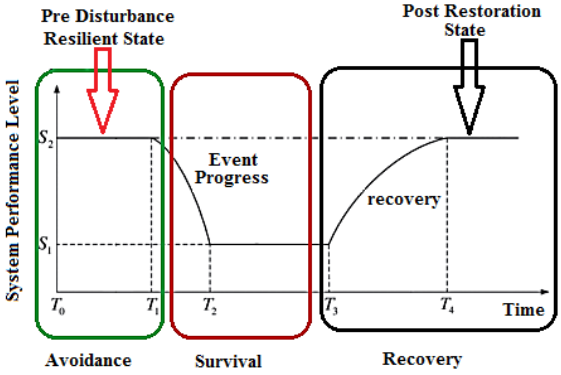

Fig. 1. The system resiliency curve and its various steps

A large number of studies have been conducted on the resilience in the distribution network and its improvement methods. For example, [2] assessed the strategies for improving the resilience in the distribution network utilizing a multivariate statistical model. In addition, [3] proposed a quantitative criterion to calculate resilience in the network applying graph theory considering different criteria for resilience through the index aggregation algorithm and the weighting factor for each index. Further, [4] focused on the role of networked microgrids (MGs) to increase the resilience in the system against extreme events. Furthermore, [5] presented an integrated and coordinated optimization model for restoring unbalanced distribution systems after large-scale power outages created by extreme events with the presence of

DOI: 10.22034/tjee.2023.55940.4604

dispatchable and renewable (solar and wind units) distributed generation resources (DGs) and ESSs. In another study, [6] offered the planning of MGs to strengthen the network against extreme events in order to determine the optimal nodes for MG connection, along with the capacity of dispatchable production units located in MGs. An optimization model was reviewed in [7] to allocate emergency power resources among the MGs and sensitive loads in a distribution system before a severe natural disaster. In addition, [8] presented a MG formation model based on emergency operation strategy for resilient distribution systems. Further, [9] proposed a second-order mixed-integer programming model using supporting DGs and reconfiguration of the distribution network to offer minimal improved load shedding to provide the resilience in the distribution network. Furthermore, [10] introduced a coordinated model to improve the resilience in the system and upgrade the operation of smart MGs in the form of resistant islanding, in which the islanding algorithm was utilized to increase resilience. In another study, [11] discussed the effect of the type, location, and optimal size of DG on the resilience in the distribution network with the help of a new resilience index. A qualitative assessment structure of resilience under stormy weather conditions for the power system was proposed in [12].

Analysing electricity and gas multi-energy systems (MESs) is considered as more complicated. However, the above-mentioned systems should not be ignored due to their interdependence because such factor may make the whole system more vulnerable, resulting in spreading the failure from one energy network to another. Applying dynamic and optimal interaction between the aforementioned energy carriers can improve the level of resilience and maximize the amount of energy supply to consumers due to the dispersion of dependent sources of electricity and gas energy networks and storages [13]. The exact method of analysing the resilience of gas networks in power systems was assessed in [14]. To this aim, the constraints related to gas infrastructures were evaluated considering different thermal scenarios. The proposed model was based on a multi-stage method which uses DC load flow, as well as stable and transient analyses for power systems and gas networks, respectively. Then, the effects of electricity and gas networks on each other were examined by offering a new criterion to measure the provided resilience. The results indicated that the proposed method exhibits an effective perspective on the effects of the thermal energy network on the resilience of MESs. An economic dispatch model was proposed as a multi-level problem considering security constraint. The interaction between the electric grid and natural gas was regarded in the proposed model, along with wind power and the convert electricity to gas unit. Therefore, utilizing different energy carriers during the planning can increase the resilience in energy supply systems significantly. The expansion planning algorithm was proposed for energy transmission systems resulting from the integration of electric and gas networks to increase the resilience of the network in difficult conditions [15].

In [16], the rate of frequency change has been utilized as a new indicator to assess system resilience during severe events. In this regard, the dispatch strategy of distributed generation units has been employed as an optimal solution to mitigate sudden generator outages and prevent frequency instability.

With the restructuring of electricity networks and motion towards smart electric networks, microgrids will play a significant role in ensuring network critical loads [17, 18]. MGs can play a significant role in improving resilience in energy distribution systems. In fact, MGs can be immediately connected to the critical buses of the network in an island performance in the event of a disruption in the energy supply in an electrical energy distribution system. The significance of timing and sequence of events in the proactive management approach can prevent delays in emergency power supply appropriately. An optimal MG scheduling model was offered in [19] to improve the resilience and minimize the reduction of MG load interruption in islanding operation. In addition, [20] applied a two-stage stochastic programming approach to find the optimal MG scheduling under uncertainty. DGs in MGs maintain the continuity of feeding loads for consumers and critical loads after extreme events, which plays a significant role in resilience [21]. Further, [22] investigated various topics related to MG control and restoration with their help to strengthen network resilience. Furthermore, [23] presented a resilience-based approach with the help of MG to restore critical loads in a distribution feeder after a major natural disaster. In another study, [24] focused on the risk limitation strategy using MGs based on a Gaussian hybrid model to express the quantitative assessment of resilience in terms of the probability distribution of wind turbine and photovoltaic production to restore the load. A hierarchical blackout decision-making model was utilized in [25] to control multi-MGs (MMGs) intelligently in order to increase the resilience in smart grids.

Based on the studies, the interdependence in natural gas network infrastructure with the presence of compressors and electricity distribution network is ignored. This study aims to allocate the above-mentioned resources in the system before the storm. The objective of this research is to enhance the level of resilience based on proactive scheduled management by incorporating microgrids as resilient resources and utilizing the storage capacity within them to improve resilience prior to the occurrence of severe events in the avoidance phase, as shown in the resilience curve in Fig. 1. During this time interval, certain initial potential events, including warning time, gas outages, and system islanding, are identified for a specific distribution system. With this information, by optimizing the defined objective functions that involve maximizing the level of system storage devices and minimizing the amount of lost load while ensuring critical loads, we maximize the level of non-critical load supply. Finally, the system resilience index is determined based on the obtained information. Therefore, considering the provided explanations, the objective of this article is not optimal energy management in an islanded microgrid but rather the maximization of energy storage levels during the period of renewable source outage and gas interruption by predicting the occurrence of severe events. The proposed model is regarded as a non-linear programming problem optimized by MOACO. The remainder of this study is as follows. The proposed plan

DOI: 10.22034/tjee.2023.55940.4604

and its relationships are indicated in the second part. The third part focuses on the proposed model which is implemented in an integrated system including electric and gas networks and utilized to analyze the resilience in the network. Finally, the conclusion is reviewed.

2. The Proposed Methodology

A proactive scheduled management program is aimed at delaying or reducing the system's vulnerability prior to the occurrence of an event. Considering that it is possible to predict a severe event such as a storm several hours before its occurrence, this paper considers the possibility of predicting the accessible energy storage capacity in a microgrid prior to an event as a preventive principle. This approach aims to maximize the energy storage capacity and increase the network's resilience level. Fig. 2 illustrates the flowchart of the proposed plan, demonstrating the three stages of the overall process of implementing the active scheduling management approach.

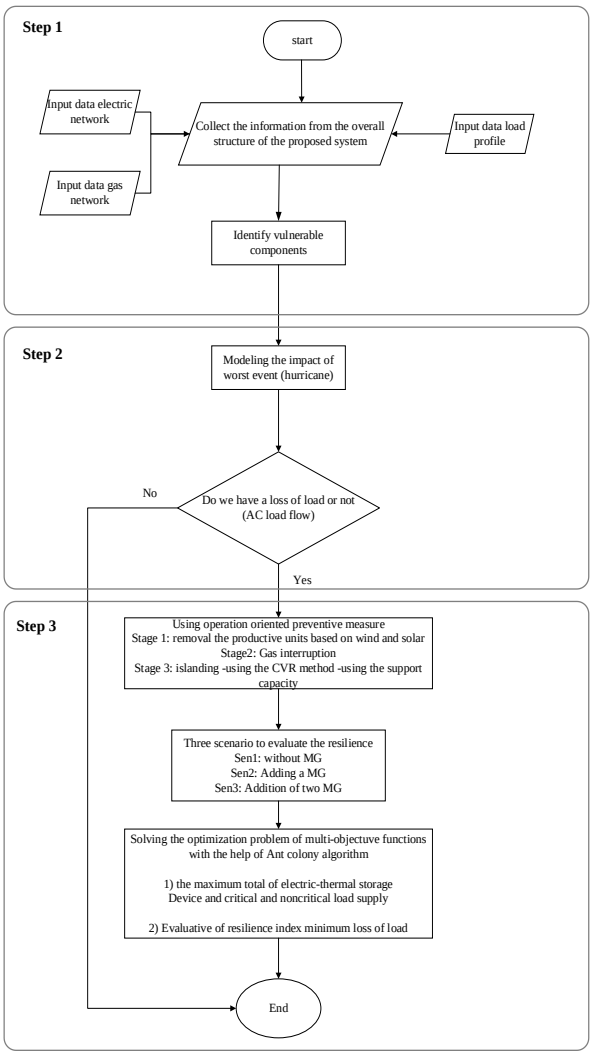

Fig. 2.The flowchart of the proposed scheme

A very important point in this research is the time interval considered for evaluating the system's behavior. According to Fig.1, the time interval from T0 to T1 represents the phase of providing an appropriate scheduling plan to achieve the maximum energy storage level before the occurrence of a severe event at time T1. In practice, within the time interval from T0 to T1, according to the provided schedule, the outage of renewable sources and gas interruption occurs. At time T1, the modeling phase of vulnerable elements such as feeders and transformers based on the occurrence of a severe event takes place. The candidate equipment for potential damages in the face of severe events such as storms are feeders, transformers, and renewable sources like wind and solar. In the proactive scheduling plan, initially, the sources are disconnected from the network at the time of the initial alert announcement. The next step is to select the worst weather condition based on. statistically predicted data aligned with the wind speed in the geographical area.

3. Formulating the Problem

The characteristics of the interconnected electricity and natural gas distribution network are formulated based on several scenarios considering MGs.

3.1 Electric network equations

3.1.1 electric power flow

Equations (1-4) are related to AC power flow.

$$\sum_{n\in\Omega} P_{n,t}^{G,e} - \sum_{n\in\Phi}(P_{a,t}^{es+,e} - P_{a,t}^{es-,e}) - P_{i,t}^{cl,e} - P_{i.t}^{s,ncl,e} = P_{i.t}^{inj} \quad (1)$$

$$\sum_{n\in\Omega 1} Q_{n,t}^{G,e} - Q_{i,t}^{cl,e} - Q_{i.t}^{s,ncl,e} = Q_{i.t}^{inj} \quad (2)$$

where $P_{n,t}^{G,e}$ and $Q_{n,t}^{G,e}$ indicate the variables of active and reactive electric and boiler power and $P_{a.t}^{es+,t}$ and $P_{a,t}^{es-,t}$ represent the charging and discharging capacities of electric storages, respectively.

$$P_{i,t}^{inj} = (2V_{i,t} - 1)G_{(i,t)}^{y} + \sum_{j(j\neq i)}^{N_{e-bus}} (G_{(i,j)}^{y}(V_{i,t} + V_{j,t} - 1) + B_{(i,t)}^{y}(\theta_{i,t} - \theta_{j,t})) \quad (3)$$

$$Q_{i,t}^{inj} = -(2V_{i,t} - 1)B_{(i,t)}^{y} + \sum_{j(j\neq i)}^{N_{e-bus}} (-B_{(i,j)}^{y}(V_{i,t} + V_{j,t} - 1) + G_{(i,t)}^{y}(\theta_{i,t} - \theta_{j,t})) \quad (4)$$

The variables $P_{i,t}^{inj}$ and $Q_{i,t}^{inj}$ are regarded as the active and reactive powers injected in each bus and the parameters G^{y} and B^{y} are considered as the real and imaginary parts of the admittance matrix, respectively. The limit of power exchange with the upstream network is as follows.

$$(P_t^{grid})^2 + (Q_t^{grid})^2 \le (U_t^{grid} S_{\max}^{grid})^2 \quad (5)$$

Where S_{max}^{grid} indicates the apparent power of the substation, P_t^{grid} and P_t^{grid} represent the active and reactive power of the substation, U_t^{grid} and demonstrates the connection status of the MES system. Zero means the connection is regarded as island and one indicates the connection to the network. The upper and lower limits or limits of the voltage are as follows:

DOI: 10.22034/tjee.2023.55940.4604

$$\underline{V}_i \le V_{i,t} \le \overline{V}_i \quad i \ne substation-bus \tag{6}$$

$$U_t^{grid} V_o + (1-U_t^{grid})\underline{V}_i \le V_{i,t} \le U_t^{grid} V_o + (1-U_t^{grid}) V_i \quad i = substation-bus \tag{7}$$

The aforementioned equations indicate the limit of the maximum active and reactive production power in each DG [26]. In addition, Equation (10) is considered to limit the active production power of the sources during the fault period because some DGs may face obstacles in supplying their fuel after an extreme event.

$$P_{n,t}^{DG} \le \sum_{k\in k} \alpha_{i,t}.P_n^{DG,\max} \tag{8}$$

$$\sum_{k\in k} \alpha_{i,t}.Q_n^{DG,\min} \le Q_{n,t}^{DG} \le \sum_{k\in k} \alpha_{i,t}.Q_n^{DG,\max} \tag{9}$$

$$\sum_{t\in T}\sum_{m\in M} P_t^{DG} \le E^{DG,total} \tag{10}$$

The limits of reducing electrical loads are as follows.

$$0 \le P_{i,t}^{s,ncl,e} \le P_{i,t}^{s,ncl,e} \tag{11}$$

$$Q_{i,t}^{s.ncl.e} = Q_{i,t}^{ncl.e} - (P_{i,t}^{ncl.e} - P_{i,t}^{s.ncl.e}).(\frac{Q_{i,t}^{ncl.e*}}{P_{i,t}^{ncl.e*}}) \tag{12}$$

Where $P_{i,t}^{s,ncl,e}$ and $Q_{i,t}^{s,ncl,e}$ indicate the active and reactive power of non-critical electrical demand, respectively.The limit of line power distribution is displayed in Equations (13) and (14).

$$P_{(i,t).t}^{fl.e} = G_{(i,t)}^{l} - (V_{i,t} - V_{j,t}) - B_{(i,t)}^{l}(\theta_{i,t} - \theta_{j,t}) \tag{13}$$

$$P_{(i,j).t}^{fl.e} + P_{(j,i).t}^{fl.e} \le \overline{P}_{(i,j)}^{loss} \tag{14}$$

Where $P_{(i,j),t}^{fl,e}$ is considered as the active power flow of line, $P_{(i,t)}^{loss}$ is regarded as the active power loss of feeder, and the parameters G^l and B^l indicate conductance and susceptance of the line, respectively. The line current limit is applied to the thermal capacity of the feeder in Equation (14). Therefore, the total active loads flow in two directions is related to the losses of the feeder. The MES network is connected to the upstream network at the point of common coupling (PCC), where two types of DGs are considered, one with natural gas fuel and the other with dual fuel (diesel). The dual fuel DGs burn natural gas due to the environmental and economic advantages of natural gas compared to diesel. The limitations of operator DGs are as follows.

$$\alpha_{n,t}\underline{P}_n^{G.e}\gamma_n \le P_{n,t}^{G.e} \le \alpha_{n,t}\overline{P}_n^{G.e}\gamma_n \tag{15}$$

$$\alpha_{n,t}\underline{Q}_n^{G.e}\gamma_n \le Q_{n,t}^{G.e} \le \alpha_{n,t}\overline{Q}_n^{G.e}\gamma_n \tag{16}$$

where the variable γ_n indicates the state status of DGs. Accordingly, this value is equal to one when DGs are in service and otherwise they are zero. The natural gas fuel sources exit from the circuit and the units of dual fuel DGs work with gasoline when the natural gas is interrupted. The above-mentioned process is observed in Equation (17), where $\alpha_{n,t}$ and U_t^{gas} represent the state of DGs dependent on fuel and condition of natural gas, respectively. In fact, the available gas equals to one and the interrupted one equals to zero.

$$\alpha_{n,t} = \begin{cases} U_t^{gas} & n\in\Gamma \\ 1 & n\in\wedge \end{cases} \tag{17}$$

3.1.2 Electric load model

An appropriate electric load model is necessary condition to utilize the conservative voltage regulation (CVR) method. CVR controls distribution voltage levels in the range lower than the limit to reduce peak demand and energy consumption, especially in emergency situations [27] . Thus, CVR provides a proven energy source to improve the resilience of MGs during island operations. To this aim, the range of CVR is considered between 0.95-1.05. A polynomial load model known as the ZIP is applied to describe the dependence of the load on the voltage value [28].

$$P_i^L = P_i^{L*}(K_i^{PZ}(V_i/V_i^*)^2 + K_i^{PI}(V_i/V_i^*) + K_i^{PP}) \tag{18}$$

$$Q_i^L = Q_i^{L*}(K_i^{QZ}(V_i/V_i^*)^2 + K_i^{QI}(V_i/V_i^*) + K_i^{QP}) \tag{19}$$

where K_i^{PZ} indicates the contribution coefficients of impedance, while K_i^{PI} and K_i^{PP} represent the current and constant power in the active power load, respectively. In addition, K_i^{QZ} is considered as the contribution coefficients of impedance, while K_i^{QZ} and K_i^{QP} are regarded as the current and constant power in the active power load, respectively. Equation (2) shows the constraints related to the amount of production and the minimum time of microturbines being on or off.

$$P_{MT}^{\min} \le P_{MT} \le P_{MT}^{\max} \tag{20}$$

where K_i^{QP} indicates the power produced by the micro turbine, while K_i^{QP} and P_{MT}^{max} represent its minimum and maximum produced power. The MGs are controlled and started by droop control in the island mode. Therefore, the frequency of the steady state system is among the variables of load distribution. The following two equations can be presented for each DER controlled by Droop [29].

$$\omega = \omega_i^{ref} - m_i^q Q_i^G . \forall_i \in B_{droop} \tag{21}$$

$$V = V_i^{ref} - n_i^q P_i^G . \forall_i \in B_{droop} \tag{22}$$

3.1.3 Electric storage model

The state of charge (SOC) at any moment is displayed by Equation (23).

$$SOC_{a.t}^e = SOC_{a.(t-1)}^e + \frac{\eta_a^{es.e} P_{a.(t-1)}^{es+.e}.\Delta t}{\overline{E}_a^{es.e}} - \frac{P_{a.(t-1)}^{es-.e}.\Delta t}{\eta_a^{es.e}\overline{E}_a^{es.e}} \tag{23}$$

Equation (24) indicates the initial values of SOC, Equation (25) represents the depth-of-discharge (DOD), and Equations (26) and (27) display the limitations of charging and discharging power related to storage units in MES.

$$SOC_{a.(ini)}^e = SOC_a^{ini,e} \tag{24}$$

DOI: 10.22034/tjee.2023.55940.4604

$$\underline{SOC}_a^e \le SOC_{a.t}^e \le \overline{SOC}_a^e \quad (25)$$

$$0 \le P_{a.t}^{es+,e} \le \overline{P}_a^{es+,e} \mu_{a.t}^e \quad (26)$$

$$0 \le P_{a.t}^{es-,e} \le \eta_a^{es.s} \overline{P}_a^{es-,e} (1-\mu_{a.t}^e) \quad (27)$$

where P_{MT}^{max} , $\eta_a^{es,e}$, $P_t^{es\pm,e}$, and $E_a^{es,e}$ indicate the charging state of the scheduled electrical units, conversion efficiency coefficient of the electrical storage units, scheduled charging and discharging powers, and capacity of electric storage unit, respectively. Further, μ^e is considered as the scheduled charging status of the electric storage unit, which is in the charging and discharging states when it equals to one and zero, respectively.

3.2 Thermal load model

3.2.1 Thermal power distribution

Equations (28-30) are demonstrated as follows, where $P_{i,t}^{cl,h}$ is considered as the active power of critical thermal demand, while $P_{i,t}^{cl,h}$ and $P_{d,t}^{es-,h}$ are considered as the charging and discharging powers of the thermal storages, respectively. In addition, the parameters C^{o-e} , C^{o-e} , C^{g-e} , and C^{g-h} indicate the efficiency of converting gas and diesel into heat and electricity in CHPs. Further, $P_{n,t}^{G,e}$ and $P_{b,t}^{G,h}$ represent the variables of active electrical and thermal power of the boiler.

The limitation in reducing the heat load is shown in Equation (29).

The limitation in operation and production of boilers are displayed in Equations (30) and (31).

$$\begin{aligned} &P_{i.t}^{s.ncl.h} + P_{i.t}^{cl.h} + \sum_{d\in K_i} (P_{d.t}^{es+,h} - P_{d.t}^{es-,h}) = U_t^{gas} \\ &\sum_{n\in\Omega_i} (C_n^{g-h}) P_{n.t}^{G.e} / (C_n^{g-e}) \\ &+(1-U_t^{gas}) \sum_{n\in\Lambda_i} (C_n^{o-h}) P_{n.t}^{G.e} / (C_n^{o-e}) \\ &+U_t^{gas} \sum_{b\in\Upsilon_i} P_{b,t}^{G,h} + \sum_{b\in\psi_i} P_{b,t}^{G,h} \quad \forall_i \in \theta \end{aligned} \quad (28)$$

$$0 \le P_{i.t}^{s,ncl,h} \le P_{i.t}^{ncl,h} \quad \forall_i \in \theta \quad (29)$$

$$0 \le P_{b.t}^{G,h} \le X_{b.t} P_b^{-G,h} \quad (30)$$

$$X_{b.t} = \begin{cases} U_t^{gas} & b\in\gamma \\ 1 & b\in\psi \end{cases} \quad (31)$$

where the parameter $X_{b,t}$ determines the operation of the boiler dependent on the fuel. In addition, U_t^{gas} in Equation (35) displays the state of natural gas in MES. Like DGs, two models are offered in boilers with natural gas and dual fuels. The capacity of the boiler used here is 30 kW hypothesizing that dual fuel boilers normally burn natural gas and work with diesel when natural gas is interrupted. The natural gas is regarded as the fuel of the boiler. Equation (32) presents the output power in terms of boiler input fuel.

$$Q_{boiler}(t) = \eta_{boiler} \times C_{in}(t) \quad (32)$$

3.2.2 Thermal storage model

The constraints of thermal storage are demonstrated in Equations (33-37).

$$SOC_{d,t}^h = SOC_{d.(t-1)}^h + \frac{\eta_d^{es.,h} P_{d.(t-1)}^{es+,h} .\Delta t}{\overline{E}_d^{es,h}} - \frac{P_{d.(t-1)}^{es-,h} .\Delta t}{\eta_d^{es,e} \overline{E}_d^{es,h}} \quad (33)$$

$$SOC_{d.(ini)}^h = SOC_d^{ini,h} \quad (34)$$

$$\underline{SOC}_d^h \le SOC_{d,t}^h \le \overline{SOC}_d^h \quad (35)$$

$$0 \le P_{d,t}^{es+,h} \le \overline{P}_d^{es+,h} \mu_{d,t}^h \quad (36)$$

$$0 \le P_{d,t}^{es-,h} \le \eta_d^{es,h} \overline{P}_d^{es+,h} (1-\mu_{d,t}^h) \quad (37)$$

where SOC_d^h indicates the charging state of the scheduled thermal units and the parameter $\eta_d^{es,h}$ represents the conversion efficiency coefficient of the thermal storage units. In addition, the variable $P_d^{es+,h}$, $P_d^{es-,h}$ is considered as the charging and discharging capacities of the thermal storages and the parameter $E_d^{es,h}$ is regarded as the capacity of the thermal storage unit. Further, μ^h represents the scheduled charging state of the thermal storage unit, which is in the charging and discharging states when it equals to one and zero, respectively.

3.3 Natural gas network equations

Loads in the natural gas network include DGs, boilers, and residential/industrial natural gas loads. The balance of natural gas and its limitation for a gas node are expressed as Equations (38) and (39).

$$\begin{aligned} &\sum_{u\in H_k} \upsilon_{u.t}^g - D_{k,t}^g - U_t^{gas} \sum_{n\in I_k} P_{n,t}^{G,e} \rho_n^{g-e} - \\ &U_t^{gas} \sum_{b\in E_k} P_{b,t}^{G,h} \rho_b^{g-h} = \sum_{m(m\neq k)}^{N_{g-node}} fg_{(k,m),t} \end{aligned} \quad (38)$$

$$U_t^{gas} .\underline{\upsilon}_u^g \le \upsilon_{u.t}^g \le U_t^{gas} .\overline{\upsilon}_t^g \quad (39)$$

where the parameter $D_{k,t}^g$ indicates the gas demand, while the parameters ρ_n^{g-e} and ρ_b^{g-h} represents the natural gas consumption rate of DG and steam boiler, respectively. Distributing natural gas flow in each distribution pipeline and natural gas pressure constraint are expressed by Equations (40) and (41), respectively.

$$sign(fg_{(k.m).t}) fg_{(k.m).t^2} = c_{(k.m)}^{p^2} (ps_{k.t^2} - ps_{m.t^2}) \quad (40)$$

where $c_{(k,m)}^{p^2}$ is considered as the pipeline constant.

$$\underline{ps} \le ps_{k.t} \le \overline{ps} \quad (41)$$

DOI: 10.22034/tjee.2023.55940.4604

Diesel storage limitations: Diesel is stored in this system to supply DGs and dual fuel boilers. Obviously, such storage has limitations in the form of Equations (42) and (43).

$$v_{i.t}^{o} = v_{i.(t-1)}^{o} - (1-U_{(t-1)}^{gas}) \sum_{n\in\Lambda_i} P_{n.(t-1)}^{G.e} \rho_n^{o-e} - (1-U_{(t-1)}^{gas}) \sum_{b\in\Psi_i} P_{b.(t-1)}^{G.h} \rho_b^{o-h} \quad (42)$$

The parameters $\rho_n^{o\text{-}e}$ and $\rho_b^{o\text{-}h}$ indicate the gas consumption rate in DG and boiler.

$$v_{i.(ini)}^{o} = v_i^{o.ini}$$
$$v_{i.t}^{o} \geq 0 \quad (43)$$

3.4 the objective function description

The multi-objective function is defined as the sum of the energy stored in the electrical and thermal storage units and the non-critical load provided at the end of the avoidance stage. Thus, a multi-objective function is proposed to make a compromise between MES active readiness and pre-event load reduction according to Equations (44) and (45). Variables F1 and F2 are regarded as objective functions.

$$f_a = \sum_i \sum_t P_{i,t}^{s,ncl,e} .\Delta t + \sum_{i\in\theta} \sum_t P_{i,t}^{s,ncl,h} .\Delta t + \sum_a SOC_{d,t=N_T}^{e} + \sum_a SOC_{d,t=N_T}^{h} \quad (44)$$

$$F_1 = \max(f_a)$$

$$f_b = RI = \frac{1}{T} \sum_{i=1}^{NB} P_i^{shed} .\Delta t \quad (45)$$

$$F_2 = \min(f_b)$$

$$F = \begin{bmatrix} F_1 & F_2 \end{bmatrix} \quad (46)$$

Equation (44) indicates the sum of electrical and thermal storages, as well as supplying non-critical loads at the end of the planning horizon, and the value of *RI* in Equation (45) represents the resilience index (amount of energy loss). The variable P_i^{shed} is considered as the interrupted active power and γ_i is regarded as the weight based on load priority. Providing a certain level of energy storage at the start of the event improves the readiness of the system to supply critical loads in extreme conditions after the event. The proposed method utilizes production/storage rescheduling and CVR as OPM in the avoidance stage. An integrated power grid of natural gas and electricity based on resiliency is applied in linearization method which can model natural gas interruption and islanding event.

The system operator should accept the responsibility for the integrated energy system due to the interdependencies inherent in MES. Finally, the results can be practically used by the MES operator to apply preventive set points by which the system can be prepared against the future event (opening of the uncertainty interval). System operators should start preventive measures early to avoid power outages and possible failures due to the spatial and temporal characteristics of the events and the rapid change in the state of the components. Table 1 indicates an event chain with a 12-hour planning horizon which affects the network in the form of scheduling the events with clear critical times. The prevention stage is defined from the first announcement of a storm warning to the first moment which it may enter the MES system. Then, a coordinated preventive method is utilized to eliminate the adverse effects of the storm. The operator removes natural gas platforms and all of the wind-based production resources before the event conservatively in order to observe safety measures and predict the path of the storm.

Table 1. Range of consecutive time events

Time	Status
t_0 =8	Storm early warning
t_1 =12	Natural gas cut
t_1 to t_2	Identification of storm-exposed airways and removal of wind-based resources
t_2 =17	Island mode (disconnecting from the upstream network)
t_3 =20	The beginning of the storm
t_3 to t_4	The occurrence of a storm

DERs and natural gas boilers experience a forced shutdown when the supply of natural gas in MES is interrupted, resulting in losing a part of the demand for electricity and heat. In order to maintain the resilience of the power grid and prevent possible outages, the power system operator forces the MES to work in island mode as a preventive decision. In fact, the MES operator is already informed of the relevant time moments (t_1 and t_2) in t0 since the natural gas interruption and the island event occur as preventive decisions by the operators in the natural gas network and upstream electricity network.

The proposed MG resilient design problem is based on a non-convex and mixed integer linear optimization problem, solving of which requires a powerful optimization algorithm. The objectives of the problem in multi-objective optimization are sometimes contradictory or in competition with each other. In addition, a set of optimal solutions is produced instead of providing an optimal one. The set of optimal solutions, which is called Pareto optimality, as well, includes answers which exhibit no superiority to each other considering all of the objectives. The MOACO algorithm is among the meta-heuristic methods based on population and is regarded as a constructive technique for finding approximate solutions to difficult optimization problems. The MOACO algorithm aims to solve the problem by searching for a path with minimum cost in a graph. Determining the input vector for the variables related to intelligent algorithms correctly is among the most significant parts of problem modeling. The following steps are proposed for the resilience based on proactive preventive management plan in multi-energy carrier distribution network by the MOACO algorithm.

Pheromone: Two strategies are applied for calculating the amount of pheromone in the algorithm.

A. A pheromone matrix (optimal capacity of DG and load flow in the distribution network) is considered and sum of the objective functions (maximizing the energy level in the storages in the network and the minimum amount of load loss) is used for its calculation.

DOI: 10.22034/tjee.2023.55940.4604

B. One colony and one pheromone matrix are regarded for each objective function (maximizing the energy level of the storages in the network and minimizing the amount of load loss).
Selecting the answer: The appropriate solution is among the issues arising during updating the value of pheromone routes. Two methods are utilized to select the optimal solution.
A. What is the best solution for each objective function?
B. What are the non-superior solutions?
Exploratory factors: In order to define this factor, two strategies are applied.
A. Considering the sum of the objective functions (maximizing the energy level of the storages in the network and the minimum amount of load loss).
B. Considering a colony for each objective function (maximizing the energy level of the storages in the network and the minimum amount of load loss).
The parameters of the MOACO algorithm are obtained using the trial-and-error method. The number of ants, pheromone evaporation coefficient, probability of mutation, and percentage of elites equal to 200, 0.6, 0.4, and 0.1, respectively.

4. Proposed test system and simulation results

A modified IEEE 33-bus test network is considered Fig. 2. which is connected to a 14-node gas system.

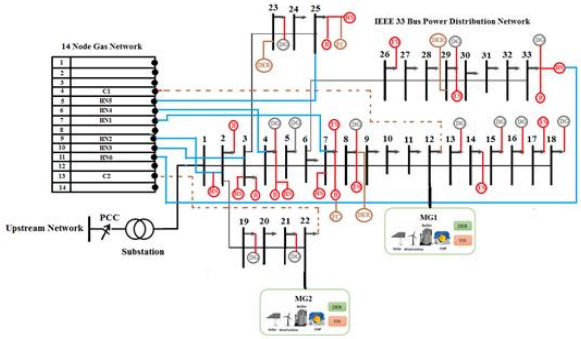

Fig. 3. IEEE 33 bus test network

To generate electricity, the distribution network depends on the gas network, which has two compressor stations and consumes electricity to operate its compressors. There are two compressors in nodes 4 and 13, which help by maintaining a constant pressure in the gas transmission pipelines from one node to another one. The compressors are supplied by the power supply located in buses 12 and 22 of the power network. The upper and lower limits in the capacity of nodes are 61.1 and 28.6 m^3, and those of natural gas pressure in the distribution network are 4.13 and 3.45, respectively. The priority for all of the network loads is considered as equal and the daily load profile is regarded as the same for all of the loads. The electrical and thermal efficiency of CHP equal to 0.33 and 0.5, respectively. The proposed method is evaluated in island mode by interrupting the common connection at the PCC point (where the MES network is connected to the upstream network) and the preventive scheduling lasts 12 hours. There are six nodes in the thermal system, each of which includes some thermal loads, boilers, thermal storage unit, and CHP units. The available resources of MGs are assumed to supply the entire system load in the island mode and MGs can be successfully connected to the network without any obstacles such as failure of components or buses. In addition, no performance losses is considered after connection by MGs. To assess the effect of the MGs, their connection is randomly done to a bus which depends on the gas network. Here, three scenarios are considered to evaluate the resilience.
(1) The presence of MGs is not considered in the first scenario.
(2) The second scenario, MG1 is randomly added to a damaged bus in the power network (bus 12 or 22) that has buses corresponding to the gas network.
(3) The third scenario is implemented to add the second MG to the gas-electricity network. As shown in Figure 2, the second MG is randomly connected to bus 22 of the power grid.
In this paper, a maximum sustained wind speed of approximately 35 meters per second has been considered [30 31].” Other vulnerable equipment is obtained by plotting the equipment fragility curve, as shown in Fig. (4), based on the maximum predicted wind speed according to the relationship (47).

$$P_b(w) = P_{b,l}(w) + P_{b,T}(w) - P_{b,l}(w) \times P_{b,T}(w) \quad (47)$$

Where the probability of branch outage, , due to feeder or transformer failure, , is a function of wind speed. In this study, a vulnerability threshold of 5% is assumed for each distribution network branch. In the next step, based on the worst possible scenario, which includes the outage of all identified vulnerable components in the previous section, the optimal AC power flow program is executed to determine the amount of lost load in the system.
Based on the vulnerability threshold assumed to be 5% for each branch of the distribution network, in this study, branches 11-12, 7-8, 2-3, 5-6, 14-15, 21-22, 6-26, and 30-31 have been identified as vulnerable branches in this system.
Table 2 shows the data related to DGs and electrical and thermal storage units and boilers.
Fig. 5 displays the production profiles of electric power during the planning horizon in the proposed proactive method. As shown in Fig. 6, boilers and DGs with natural gas fuel no longer work and dual fuel boilers with diesel fuel operate limitedly from the time of natural gas interruption in period 7 (t_1=14). The production power entered from the upstream network becomes zero from the island state onwards, which is in period 10 (t_1=17).

Table 2. Data related to DGs and electrical and thermal storage units

DOI: 10.22034/tjee.2023.55940.4604

Fig. 7 is related to the thermal power production profile of steam boilers during the planning horizon in the proposed proactive method in the three specified scenarios and it shows the increase of production values of thermal power of boilers with the presence of microgrids.

Distributed Generation (DGS)						
DGs	BUS	TYPE	P_n^{-G} (MW)	P_{-n}^{G} (MW)	Q_n^{-G} (MVAR)	Q_{-n}^{G} (MVAR)
1	5	Bi-Fuel	3	0.3	2.5	-2.5
2	8	CHP,Bi-Fuel	4	0.4	3	-3
3	13	CHP,Gas-Fired	1	0.15	0.8	-0.8
4	16	CHP,Bi-Fuel	1	0.15	0.8	-0.8
5	19	Bi-Fuel	3	0.3	2.5	-2.5
6	21	CHP,Gas-Fired	3	0.25	2.5	-2.5
7	23	CHP,Bi-Fuel	2	0.2	1.6	-1.6
8	29	Gas-Fired	2	0.2	1.6	-1.6
9	33	CHP,Bi-Fuel	2	0.2	1.6	-1.6
10	15	Bi-Fuel	3	0.3	2.5	-2.5
11	18	CHP,Bi-Fuel	4	0.4	3	-3
12	4	CHP,Gas-Fired	3	0.25	2.5	-2.5

Thermal Storage (HS)					
HS	**HN**	**Capacity (MWh)**	P_d^{-ES} (MW)	SOC_d (%)	η_d^{ES}
1	HN1	3	1	30	0.9
2	HN2	1	0.25	30	0.9
3	HN3	1	0.25	20	0.9
4	HN4	2	0.5	20	0.9
5	HN5	2	0.5	20	0.9
6	HN6	1	0.25	35	0.9

Boilers				
Boiler	**HN**	**TYPE**	P_b^{-G} (MW)	P_{-b}^{G} (MW)
1	HN1	Gas-Fired	1	0.1
2	HN2	Bi-Fuel	1	0.1
3	HN3	Bi-Fuel	1	0.1
4	HN4	Bi-Fuel	2	0.15
5	HN5	Gas-Fired	1	0.1
6	HN6	Bi-Fuel	1	0.1

Electric Storage (ES)					
ES	**BUS**	**Capacity (MWh)**	P_d^{-ES} (MW)	SOC_d (%)	η_d^{ES}
1	8	6	2	30	0.95
2	14	6	2	40	0.95
3	26	4.5	1.5	20	0.95
4	7	6	2	30	0.95
5	17	4.5	1.5	20	0.95
6	29	6	2	40	0.95

Distributed Energy Resources (DER)						
DER	**BUS**	**Mode**	P_n^{-G} (MW)	P_{-n}^{G} (MW)	Q_n^{-G} (MVAR)	Q_{-n}^{G} (MVAR)
1	8	Droop	2	0.2	1.6	-1.6
2	23	Droop	1	0.2	0.8	-0.8
3	29	Droop	1	0.1	0.8	-0.8

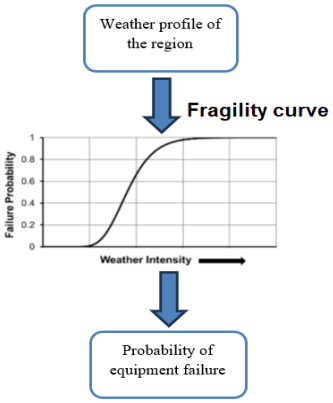

Fig.4. Equipment fragility curve

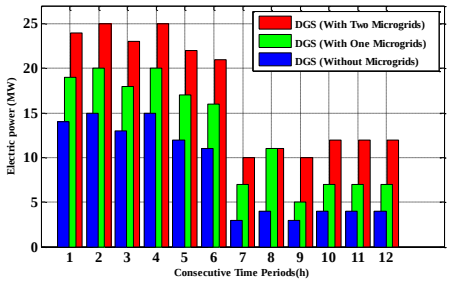

Fig. 5. Electric power production profile during the planning horizon

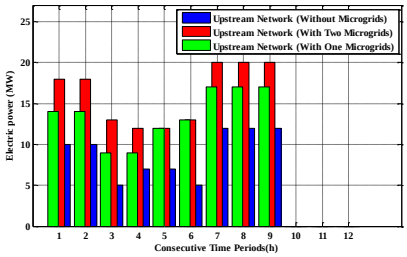

Fig. 6. Production profile of electric power from the upstream network

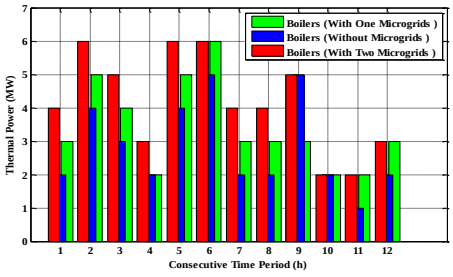

Fig. 7. Thermal power production profile during the planning horizon

Fig. 8 is related to the thermal power production profile of the simultaneous electricity and heat generation units during the planning horizon in the proposed proactive method in the three specified scenarios. As illustrated, the production values in thermal power of CHPs decrease in all of the three scenarios from natural gas interruption (time period 7) until the beginning of the islanding event in time period 10 and increase from time period 10 to 12, which means the beginning of uncertainty due to the occurrence of storm.

DOI: 10.22034/tjee.2023.55940.4604

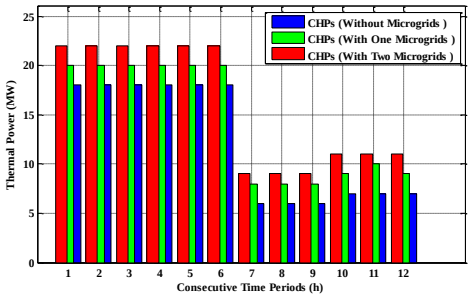

Fig. 8. Thermal power production profile during the planning horizon

The effect of CVR in the proposed proactive method is considered as a proactive instrument to control the bus voltage levels below the permissible limit, resulting in reducing the peak power consumption demand of loads in emergency situations after islanding events. Therefore, CVR provides a verified energy source for improving the resilience of MGs during island operation with an effective role in realizing the proposed model. Fig. 9 demonstrates the effect of CVR on bus voltage control. As observed, voltage reduction occurs in 10 time periods after the island event.

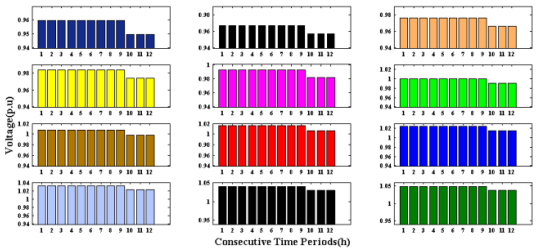

Fig. 9. Effect of CVR on bus voltage control

Based on the results, the ability of MES to provide critical loads in post-storm conditions improves when more power is stored in storage units. Figs. 10 and 11 display the relative sum of electrical and thermal storage during the planning horizon in the proposed proactive method in the scenarios determined in term of percentage. As observed, the electric storages start charging after the initial warning at 8 o'clock and maintain an appropriate level of energy storage until the end of the planning horizon and the beginning of the uncertainty. The highest percentage of energy storage is reported in the hour t_1=14 when the natural gas is interrupted by the operator.

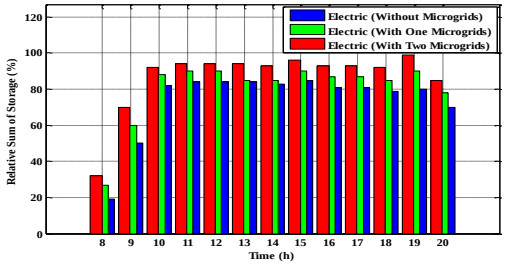

Fig. 10. Relative sum of electrical storage during the planning horizon

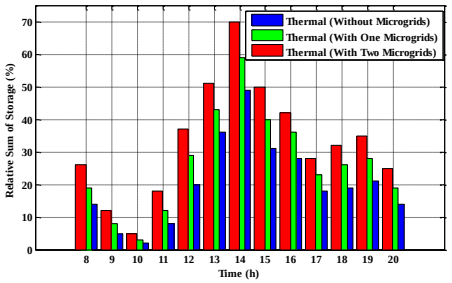

Fig. 11. Relative sum of thermal storage during the planning horizon

Practically, supplying non-critical load depends on the chain of predicted events significantly. Fig. 12 shows the percentage of non-critical load supply for electrical and thermal demands in three different scenarios hypothesizing that the critical load is fully supplied.

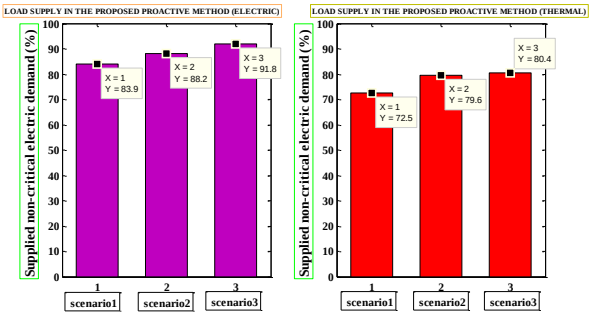

Fig. 12. Non-critical load supply percentage of electrical and thermal demand

Fig. 13 illustrates the convergence graphs for resilience index in 200 generations and in three different scenarios.

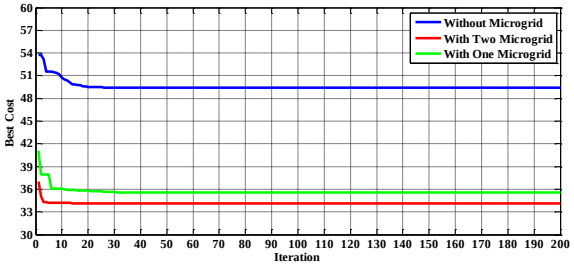

Fig. 13. Resilience index convergence diagram in three different scenarios

As represented in simulation result, the readiness index in the third scenario is higher than the first and second one, and the resilience index decreases from **49.43** in the first scenario to **35.58** and **34.16** in the second and third scenarios, respectively, indicating the better performance of the last one. To evaluate the efficiency of the multi-objective optimization algorithm of the MOACO algorithm, the rate of achieving two objective functions simultaneously (RAS) is utilized as follows.

$$RAS = \frac{\sum_{i=1}^{n} \left| f_{1i}(x) - f_{1i}^{best}(x) \right| \left| f_{2i}(x) - f_{2i}^{best}(x) \right|}{n} \quad (48)$$

where n, f_1^{best}, and f_2^{best} represent the number of non-dominant solutions, ideal value for the first objective function, and ideal value for the second objective function, respectively. Lower values for the aforementioned index indicate that the algorithm is

regarded as more efficient. The value of the above-mentioned index is 10.666.

5. Conclusion

The present study sought to examine a proactive and resilient approach to maximize the level of electrical and thermal storages, as well as non-critical load supply, while minimizing the amount loss of load since the presence of static MGs under a scheduled proactive management affects the resilience of multiple-energy carrier distribution networks significantly. The MOACO algorithm was applied for simultaneous optimization of the aforementioned objectives. The role of compressors in the gas network indicates its dependence on the electric network. Based on the results, MGs are considered as an appropriate source for improving the resilience in a short-term approach. In addition, the resilience index defined based on the amount of energy loss decreases from 49.43 in the first scenario to 34.16 in the third one, indicating the improvement of its performance. Using proactive preventive management provides a certain level of energy storage for the network before the storm arrives. No possibility of secondary failure such as load imbalance is considered. Thus, such conditions can be regarded in future works, or the energy hub structure can be utilized to analyze the resilience of the MES network instead of the above-mentioned structure.

6. References

[1] M. Panteli, D.N. Trakas, P. Mancarella and N.D. Hatziargyriou, "Power Systems Resilience Assessment: Hardening and Smart Operational Enhancement Strategies", Proceedings of the IEEE, Vol. 105, No. 7, 2017, pp. 1202-1213, http://doi: 10.1109/JPROC.2017.2691357.

[2] R. Nateghi, "Multi-Dimensional Infrastructure Resilience Modeling: An Application to Hurricane-Prone Electric Power Distribution Systems", vol. 9, no. 4, pp. 2918 – 2929, July 2018, http://doi: 10.1109/ACCESS.2018.2792680.

[3] P. Bajpai, S. Chanda, K. Srivastava, "A Novel Metric to Quantify and Enable Resilient Distribution System using Graph Theory and Choquet Integral", IEEE Trans. Smart Grid, Vol. 9, no. 4, pp. 2918 – 2929, July 2018, http://doi: 10.1109/TSG.2016.2623818.

[4] Z. Li, M. Shahidehpour, F. Aminifar, A. Alabdulwahab and Y. Al-Turki, "Networked Microgrids for Enhancing the Power System Resilience", Proceedings of the IEEE, Vol. 105, No. 7, 2017, pp. 1289-1310http://doi: 10.1109/JPROC.2017.2685558.

[5] Ye ,Z., C. Chen, B. Chen, and K. Wu. 'Resilient Service Restoration for Unbalanced Distribution Systems With Distributed Energy Resources by Leveraging Mobile Generators', IEEE Transactions on Industrial Informatics, 2021. 17: 1386-96, http://doi: 10.1109/TII.2020.2976831.

[6] Borghei, Moein, and Mona Ghassemi. 'Optimal planning of microgrids for resilient distribution networks', International Journal of Electrical Power & Energy Systems, 128: 106682.2021. https://doi.org/10.1016/j.ijepes.2020.106682.

[7] Wang, Hongbin, Yuquan Liu, Jian Fang, Jiaxing He, Yan Tian, and Hang Zhang. 'Emergency sources prepositioning for resilient restoration of distribution network', Energy Reports, 6: 1283-90,2020. https://doi.org/10.1016/j.egyr.2020.11.042.

[8] Zhu, Junpeng, Yue Yuan, and Weisheng Wang.'An exact microgrid formation model for load restoration in resilient distribution system', International Journal of Electrical Power & Energy Systems, 116: 105568,2020. https://doi.org/10.1016/j.ijepes.2019.105568.

[9] Bie, Z., Lin, Y., Li, G ,.and Li, F "Battling the Extreme: A Study on the Power System Resilience", Proceedings of the IEEE, 105 (7), pp. 1253-1266.2017. http://doi: 10.1109/JPROC.2017.2679040.

[10] M. Panteli, D. N. Trakas, P. Mancarella, and N. D. Hatziargyriou, "Power systems resilience assessment: Hardening and smart operational enhancement strategies", Proceedings of the IEEE, vol. 105, pp. 1202-1213, 2017, http://doi: 10.1109/JPROC.2017.2691357.

[11] Saberi, Reza, Hamid Falaghi, and Mostafa Esmaeeli. 'Resilience-Based Framework for Distributed Generation Planning in Distribution Networks', ieijqp, 9: 35-49. 2020.

[12] Yang, W., F. Shanshan, W. Bing, H. Jinhui, and W. Xiaoyang. 2018. 'Towards optimal recovery scheduling for dynamic resilience of networked infrastructure', Journal of Systems Engineering and Electronics, 29: 995-1008, http://doi:10.21629/JSEE.2018.05.11.

[13] Mancarella, P. “MES (Multi-Energy Systems): An Overview of Concepts and Evaluation Models”; Energy 2014, 65, 1-17.

[14] Clegg, S.; Mancarella, P. “Integrated Electrical and Gas Network Flexibility Assessment in Low-Carbon Multi-Energy Systems”; IEEE. Trans. Sustain. Energy 2016, 7, 718-731,http://doi:10.1109/TSTE.2015.2497329.

[15] Li, G.; Zhang, R.; Jiang, T.; Chen, H.; Bai, L.; Li, X. “Security-Constrained Bi-Level Economic Dispatch Model for Integrated Natural Gas and Electricity Systems Considering Wind Power and Power-To-Gas Process”; Appl. Energy 2017, 194, 696-704.

[16] M. Monemi, S. Hassanpour Darban, Unit Commitment Problem with the Aim of Increasing System Resilience, Tabriz Journal of Electrical Engineering, vol. 48, no. 4, 2018.

[17] J. Jannati, D. Nazarpour, Energy Management of Intelligent Parking lot in a Microgrid Considering the Effects of Demand Response Program, Tabriz Journal of Electrical Engineering, vol. 47, no. 2, 2017.

[18] N. Parhizi, M. Marzband, S. M. Mirhosseini Moghaddam, B. Mohammadi Ivatloo and F. Azarinejadian, “The experimental implementation of an energy management system for a grid connected microgrid by using a multiperiod imperialist competition algorithm,” Tabriz Journal of Electrical Eng., vol. 46, no. 1, 2016.

[19] Khodaei, A.. Resiliency-oriented microgrid optimal scheduling. IEEE Transactions on Smart Grid, (2014) 5(4),1584–1591, http://doi: 10.1109/TSG.2014.2311465.

[20] Gholami, A., Shekari, T., Aminifar, F., & Shahidehpour, M. Microgrid scheduling with uncertainty: The quest forresilience. IEEE Transactions on Smart Grid, 7(6), 2849–2858,2016.http://doi:10.1109/TSG.2016.2598802.

[21] Pham, T. T. H., Y. Besanger, and N. Hadjsaid. 2009. 'New Challenges in Power System Restoration With

Large Scale of Dispersed Generation Insertion', IEEE Transactions on Power Systems, 24: 398-406, http://doi: 10.1109/TPWRS.2008.2009477.
[22] Strbac, G., N. Hatziargyriou, J. P. Lopes, C. Moreira, A. Dimeas, and D. Papadaskalopoulos. 'Microgrids: Enhancing the Resilience of the European Megagrid', IEEE Power and Energy Magazine, 13: 35-43, 2015.http://doi: 10.1109/MPE.2015.2397336.
[23] Xu, Y., C. Liu, K. P. Schneider, F. K. Tuffner, and D. T. Ton. 'Microgrids for Service Restoration to Critical Load in a Resilient Distribution System', IEEE Transactions on Smart Grid, 9: 426-37, 2018.http://doi: 10.1109/TSG.2016.2591531.
[24] Wang, Z., C. Shen, Y. Xu, F. Liu, X. Wu, and C. Liu. 'Risk Limiting Load Restoration for Resilience Enhancement With Intermittent Energy Resources', IEEE Transactions on Smart Grid .22-2507 :10,2019. http://doi: 10.1109/TSG.2018.2803141.
[25] Zangeneh, Ali, Shahram Jadid, and Ashkan Rahimi-Kian. 'A hierarchical decision making model for the prioritization of distributed generation technologies: A case study for Iran', Energy Policy, 37: 5752-63. 2009.
[26] Goroohi Sardou, I., Mallahi, A., and Goroohi, A. "Optimal operation of the microgrid in presence of electric vehicles considering demand response", Iranian Electric Industry Journal of Quality and Productivity, 8(1), pp. 13-2,2019; http://doi:10.1109/TSG.2016.2594814.
[27] J. Zhao, Z. Wang, and J. Wang, “Robust time-varying load modeling for conservation voltage reduction assessment,” IEEE Trans. Smart Grid, to be published.
[28] A. Gholami, T. Shekari, F. Aminifar, and M. Shahidehpour, “Microgrid scheduling with uncertainty: the quest for resilience,” IEEE Trans. Smart Grid, vol. 7, no. 6, pp. 2849 - 2858, Nov. 2016, http://doi: 10.1109/TSG.2016.2598802.
[29] M. M. A. Abdelaziz, H. E. Farag, and E. F. El-Saadany, “Optimum droop parameter settings of islanded microgrids with renewable energy resources,” IEEE Trans. Sustain. Energy, vol. 5, no. 2, pp. 434–445, Apr. 2014, http://doi: 10.1109/TSTE.2013.2293201.
[30] M. Panteli, D. N. Trakas, P. Mancarella, and N. D. Hatziargyriou, “Boosting the power grid resilience to extreme weather events using defensive islanding.” IEEE Trans. Smart Grid, vol. 7, no. 6, pp. 2913 - 2922, Nov. 2016.
[31] A. Shafieezadeh, U. P. Onyewuchi, M. M. Begovic, and R. DesRoches, “Age-dependent fragility models of utility wood poles in power distribution networks against extreme wind hazards,” IEEE Trans. Power Deliv., vol. 29, no. 1, pp. 131–139, Feb. 2014.

7. Appendix

Indices

a	Index of electrical storage units
b	Index of thermal boilers
d	Index of thermal storage units
i, j	Indices of electric buses
k, t	Indices of natural gas nodes
n	DG index units
t	Index of time periods
u	Index of gas supply sources

Sets

Γ	A set of DGs with natural gas fuel
Υ	A set of gas boiler
Ψ	A set of dual fuel boilers
Λ	A set of dual fuel DGs
ϕ_i	A set of electrical storage units
H_k	A set of natural gas resources
E_k	A set of gas fired boilers
K_i	A set of thermal storage units
I_k	A set of gas fired DGs
Ω_i	A set of all of the DGs
θ	A set of hybrid nodes (HNs) including electrical and thermal loads.

Variables

F_1, F_2 (f_a, f_b)	Objective functions
ρs	Natural gas pressure of the gas node
V	Bus voltage size (RMS voltage)
γ	DG scheduled status
$P^{G,e}, Q^{G,e}$	Planned active and reactive powers
P^{inj}, Q^{inj}	Active and reactive powers injected in each bus
$P^{s,ncl,e}, Q^{s,ncl,e}$	Non-critical active and reactive powers supplied
$P^{cl,e}, Q^{cl,e}$	Active and reactive powers of critical electric demand
fg	Natural gas flow in the pipeline
v^g	Volume of natural gas supply sources
v^o	Volume of gasoline storage
ω	System frequency
ω_{ref}	DER output voltage frequency